

Neural-network-designed three-qubit gates robust against charge noise and crosstalk in silicon

David W. Kanaar¹ and J. P. Kestner¹

¹*Department of Physics, University of Maryland Baltimore County, Baltimore, MD 21250, USA*

Spin qubits in semiconductor quantum dots are a promising platform for quantum computing, however scaling to large systems is hampered by crosstalk and charge noise. Crosstalk here refers to the unwanted off-resonant rotation of idle qubits during the resonant rotation of the target qubit. For a three-qubit system with crosstalk and charge noise, it is difficult to analytically create gate protocols that produce three-qubit gates, such as the Toffoli gate, directly in a single shot instead of through the composition of two-qubit gates. Therefore, we numerically optimize a physics-informed neural network to produce theoretically robust shaped pulses that generate a Toffoli-equivalent gate. Additionally, robust $\frac{\pi}{2}$ X and CZ gates are also presented in this work to create a universal set of gates robust against charge noise. The robust pulses maintain an infidelity of 10^{-3} for average quasistatic fluctuations in the voltage of up to a few mV instead of tenths of mV for non-robust pulses.

I. INTRODUCTION

Spin qubits in silicon are a promising platform for creating scalable quantum computers. Current single- and two-qubit gate infidelities have been reduced to the order of 10^{-3} or below [1–7], which is under the surface code threshold [8] and is nearing the 10^{-4} threshold for CSS quantum error correcting codes [9]. Achieving similar fidelities in silicon devices with more than two qubits is challenging due to crosstalk and increased susceptibility to charge noise in these devices. Crosstalk here refers to the unwanted rotation of qubits other than the target qubit as a result of the difference in resonance frequencies between qubits not being sufficiently large compared to the driving strength (i.e. the maximum Rabi frequency).

Universal quantum computation requires a universal set of gates, for instance, single-qubit rotations and a Toffoli gate [10]. Additionally, a Toffoli gate has a classical analog and is used in many circuits for classical operations such as binary arithmetic [11, 12]. Having a direct implementation of a Toffoli gate would be faster than implementing Toffoli gates using a sequence of single- and two-qubit gates. It is, however, not straightforward to design a Toffoli gate for a chain of three exchange-coupled spins. It was shown that an equivalent gate, the iToffoli gate, can be implemented in exchange coupled spins using a pulse sequence in the absence of crosstalk [13]. Unfortunately, for a scalable silicon qubit system, it is not always possible to ignore crosstalk [14]. Methods for dealing with crosstalk for two-qubit gates have been proposed [15, 16]. However, these methods cannot be logically extended for a direct implementation of a Toffoli-equivalent gate. Furthermore, the fidelity of gates in silicon devices is limited by charge noise [17, 18] and previous methods do not correct for exchange fluctuations caused by charge noise. A method for correcting exchange fluctuations in *two-qubit* systems while considering crosstalk has previously been proposed [19]. However, this method

cannot be logically extended to a three-qubit system. Therefore, we present a shaped pulse which results in a Toffoli-equivalent gate using a physically informed neural network method originally presented in Ref. [20] and adapted to a two-qubit system in Ref. [21].

In Sec. II, the device Hamiltonian is shown and the neural network optimization method is described. In Sec. III, the pulse shapes for a non-robust iToffoli, a robust iToffoli, a robust Controlled-Z (CZ) gate, and a single-qubit $\frac{\pi}{2}$ X -rotation on the middle and outer qubits are presented. Either of the entangling gates plus the $\frac{\pi}{2}$ X -rotation, when combined with virtual- Z rotations [22], forms a universal set of gates robust against charge noise.

II. MODEL

The device we consider is a chain of three exchange-coupled spins confined in silicon quantum dots. This device in the presence of magnetic fields is well described by the Heisenberg model Hamiltonian [23] in Eq. (1).

$$H = \sum_{i=1}^3 \mu_b g_i \mathbf{B}_i \cdot \mathbf{S}_i + \sum_{i=1}^2 J_i \left(\mathbf{S}_i \cdot \mathbf{S}_{i+1} - \frac{1}{4} \right) \quad (1)$$

μ_b is the Bohr magneton, g_i is the g -factor of the i -th qubit, \mathbf{B}_i is the magnetic field at the i -th qubit, \mathbf{S}_i is the spin operator of the i -th qubit, J_i is the exchange coupling between the i -th and $(i+1)$ -th qubit. The magnetic field is applied only in the Z and X -directions and will can be described by the Zeeman energy $E_{z,i} = \mu g_i B_{z,i}$ for the Z -direction and the envelope, Ω_i , frequency, ω_i , and phase ϕ_i , $\Omega_i \cos(\omega_i t + \phi_i) = \mu g_i B_{x,i}$ for the X -direction. The rotating frame Hamiltonian, $H_R = R H R^\dagger + i\hbar(\partial_t R)R^\dagger$, in the frame $R = \exp\left(\frac{i}{2} \sum_{j=1}^3 (E_{z,j} t) Z_j\right)$ becomes

$$H_R(t) = \sum_{i=1}^3 \frac{\Omega_i}{2} \sum_{j=1}^3 \cos((E_{z,i} - E_{z,j})t + \phi_i(t))X_j + \sin((E_{z,i} - E_{z,j})t + \phi_i(t))Y_j \\ + \sum_{i=1}^2 \frac{J_i(t)}{4} [Z_i Z_{i+1} + \cos((E_{z,i} - E_{z,i+1})t)(X_i X_{i+1} + Y_i Y_{i+1}) + \sin((E_{z,i} - E_{z,i+1})t)(X_i Y_{i+1} + Y_i X_{i+1})], \quad (2)$$

which is the three-qubit extension of the two-qubit Hamiltonian in Ref. [21]. In Eq. (2) X_i , Y_i and Z_i are the Pauli operators on the i -th qubit with implied Kronecker products. Eq. (2) allows for three-tone driving, but in this work we will only use two-tone driving resonant with the outer qubits, i.e., $\Omega_2 = 0$. To demonstrate a pulse that can handle large crosstalk, the difference in Zeeman energies is chosen to be $E_{z,3} - E_{z,2} = E_{z,2} - E_{z,1} = 5\text{MHz}$ while the maximum driving strength is set to $\Omega_{\text{max}} = 10\text{MHz}$ such that they are of similar strength and the rotating wave approximation is certainly invalid. Currently, driving strengths of MHz have been implemented in experiment[2, 5, 24–27]. The maximum exchange strength was chosen to be $J_{\text{max}} = 10\text{MHz}$, which is readily attainable in experiments[4]. Additionally, the exchange will be taken to have a dependence on the barrier gate voltages V_i as $J_i = J_0 e^{2\alpha V_i}$ with $\alpha = 12.1\text{V}^{-1}$ and $J_0 = 0.056\text{MHz}$ as taken from Ref. [4]. Our methods are not specific to these choices, but we simply wish to showcase the versatility of our numerical methods to incorporate this level of experimental detail.

A. Neural network method

The large number of non-commuting terms in this Hamiltonian (2) make it very difficult to analytically create a pulse which results in a Toffoli or Toffoli-equivalent gate. Therefore, a pulse is found by numerically optimizing a physics-informed neural network using the method from Refs. [20, 21]. The sole input of this neural network is time and the outputs are the control fields $J_i(t)$, $\Omega_i(t)$, and $\phi_i(t)$. These smooth control fields are optimized to result in gates robust against charge noise in the presence of crosstalk. The DiffEqFlux.jl Julia package[28] was used to implement the neural network, the OrdinaryDiffEq.jl package [29] was used to implement the BS5 solver to solve the Schrodinger equation, and the Flux.jl and Optim.jl packages were used to implement the RADAM and BFGS optimizers to minimize the cost function consisting of two terms.

The first term in the cost function is the trace infidelity modulo virtual- Z rotations [22],

$$1-F = \min_{\vec{\varphi}} \left[1 - \frac{1}{8} \left| \text{Tr} \left(e^{\frac{i}{2}(\sum_{i=1}^3 \varphi_i Z_i)} U_c e^{\frac{i}{2}(\sum_{i=4}^6 \varphi_i Z_i)} U_t^\dagger \right) \right|^2 \right], \quad (3)$$

where U_t is the targeted evolution operator, U_c is the evolution operator produced by the control in the absence of noise, and φ_i are the virtual- Z rotation angles.

The second term in the cost function quantifies the sensitivity of the evolution operator to noise sources. For instance, a given noise will couple to the qubits via a stochastic term in the Hamiltonian, H_ϵ . The first-order Magnus expansion of the resulting noisy evolution operator is

$$U \approx U_c e^{\frac{i}{\hbar} \mathcal{E}} \quad (4)$$

where

$$\mathcal{E} = \int_0^T U_c^\dagger H_\epsilon U_c dt. \quad (5)$$

Thus, we minimize sensitivity to that noise source by including the Frobenius norm of \mathcal{E} in the cost function.

Charge noise effectively acts as fluctuations in the device voltages, which causes noise in the exchange couplings. The fluctuations in the two exchange couplings, J_1 and J_2 , are assumed to be completely uncorrelated, as this is the worst case scenario for this type of optimization [30]. This means the second term in the cost function contains the norm of the first-order Magnus expansions of both errors,

$$\mathcal{C} = (1 - F) + w \times (|\mathcal{E}_1| + |\mathcal{E}_2|) \quad (6)$$

where w is a relative weighting factor which we set to be 0.1. Minimizing only the first term in the cost function results in a gate that accounts for crosstalk in the absence of charge noise, while minimizing both terms adds robustness to charge noise. Using this method, a robust $\frac{\pi}{2}$ X rotation on the outer and middle qubit, a robust $\bar{C}Z$ gate, a non-robust iToffoli gate as well as a robust iToffoli gate are found. The iToffoli gate, iT , is a Toffoli gate that also adds an i phase for the state (or part of the state) for which the controls are met, i.e., $iT|a, b, c\rangle \rightarrow i^{ab}|a, b, c \otimes ab\rangle$ where $a, b, c \in 0, 1$. An iToffoli gate with controls on the outside qubits was chosen because it was shown in Ref. [13] to be a more natural gate for this Hamiltonian than a Toffoli gate. The driving for all cases is chosen to be two-tone driving resonant with the outer two of the three qubits.

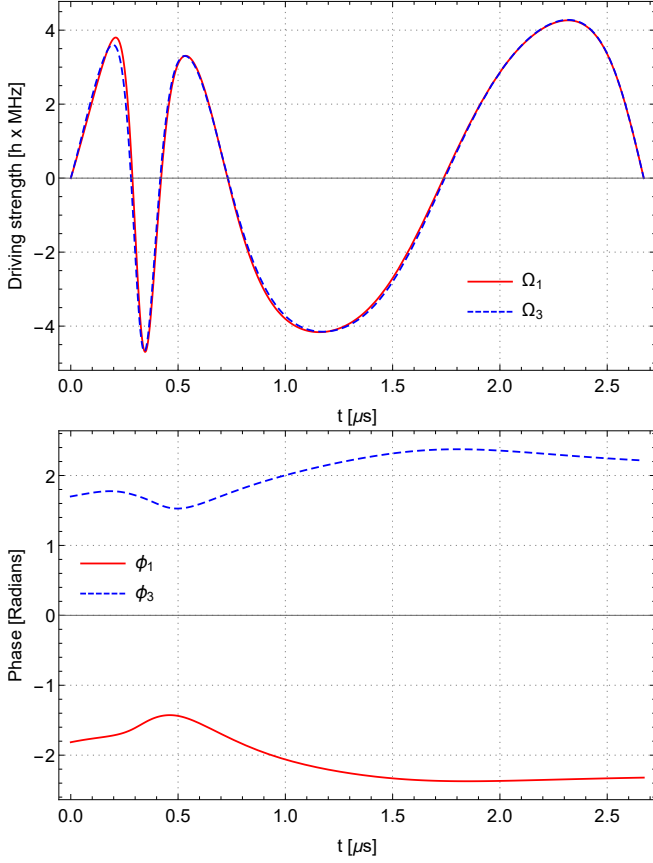


FIG. 1. Neural network designed control fields vs time for a $\frac{\pi}{2}$ X rotation on the middle qubit in the presence of crosstalk. Top: Driving tone amplitudes Ω_1 and Ω_3 . Bottom: Accompanying phase modulation of the driving ϕ_1 and ϕ_3 .

III. RESULTING GATES

A. $\frac{\pi}{2}$ X gates

Local rotations do not require any entangling, therefore the control field pulses were optimized under the constraint that the exchange be held fixed as close to zero as possible. There is always some residual coupling – here we take $J_1 = J_2 = J_0 = 0.056\text{MHz}$ [4] – but this is easily compensated for in the numerical optimization. Since the exchange is insensitive to voltage fluctuations around the uncoupled limit, any such local rotations are already trivially robust to charge noise. The optimized control field shapes for $\frac{\pi}{2}$ X rotations on the middle and outer qubits are shown in Figs. 1 and 2, respectively. They maintain an infidelity below 10^{-4} even for unrealistically large quasistatic average barrier gate fluctuations, $(\delta V_1 + \delta V_2)/2$, of 75mV (10mV) for the middle (outer) X rotation.

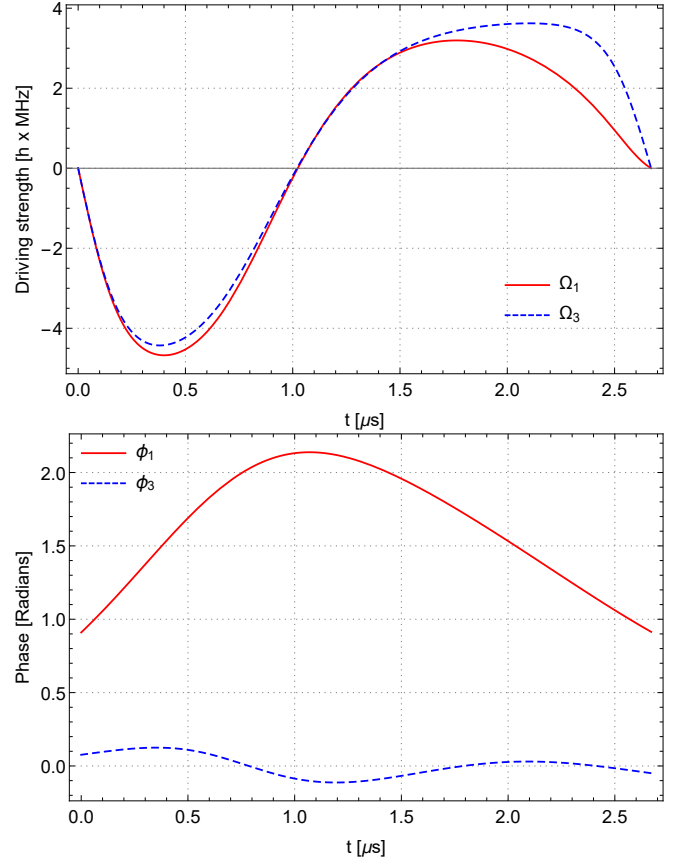


FIG. 2. Neural network designed control fields vs time for a $\frac{\pi}{2}$ X rotation on the third qubit in the presence of crosstalk. Top: Driving tone amplitudes Ω_1 and Ω_3 . Bottom: Accompanying phase modulation of the driving tones ϕ_1 and ϕ_3 .

B. CZ gate

A non-robust CZ gate is efficiently implemented adiabatically because nonadiabatic two-qubit gate fidelities are limited by the ratio of the difference in resonance frequencies to the exchange coupling strength used to implement the gate[31]. For this reason we only need to optimize for a robust CZ gate. The CZ gate on the first two qubits does not need exchange between the second and third qubit to be turned on, so we fix $J_2 = J_0$. Therefore, the gate will automatically be insensitive to fluctuations in δV_2 . The control fields of the robust CZ gate are shown in Fig. 3.

1. Charge noise analysis

The fidelity as a function of the average quasistatic fluctuation of voltages, $(\delta V_1 + \delta V_2)/2$ for all entangling gates considered are shown in Fig. 4. The CZ infidelity remains below 10^{-3} for average quasistatic voltage fluctuations up to 6.0mV. Charge noise however is not generally quasistatic but has a frequency dependence of $1/f$

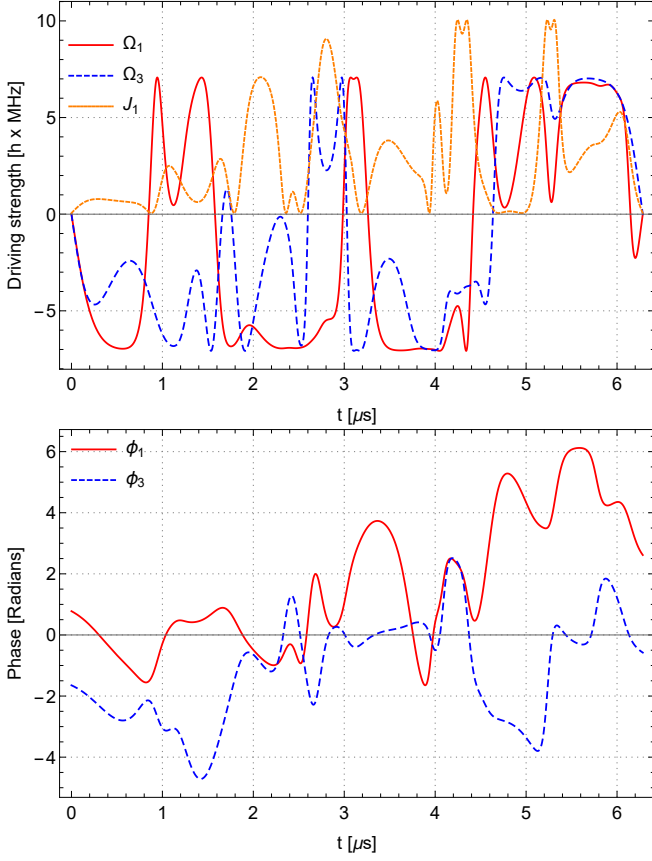


FIG. 3. Neural network designed control fields vs time for a CZ₁₂ gate in the presence of crosstalk. Top: Exchange amplitudes J_1 and J_2 as well as driving tone amplitudes Ω_1 and Ω_3 . Bottom: Accompanying phase modulation of the driving tones ϕ_1 and ϕ_3 .

between the calibration infrared cutoff, ω_{ir} and a high frequency cutoff, ω_{cutoff} , after which it falls off as $1/f^2$. To analyze the effect of time dependent charge noise we use the filter function formalism from Ref. [32]. The filter function, $\mathcal{F}(\omega)$, with our definition, is the Fourier transform of the error Hamiltonian in the toggling frame which shows the frequency response of the pulse. As voltage fluctuations are treated as uncorrelated, the gates can have separate filter functions, \mathcal{F}_i for δV_i , which are plotted in Fig. 4. The CZ gate is practically unaffected by fluctuations in δV_2 since J_2 is not driven during the pulse so only \mathcal{F}_1 is calculated and plotted. An estimate of the average infidelity is found by adding together the integral $\frac{1}{2\pi} \int_{\omega_{\text{ir}}}^{\infty} S(\omega) \mathcal{F}_i(\omega) d\omega$ for both error sources δV_i . The power spectral density, $S(\omega)$, of the charge noise induced voltage fluctuations is the same for both δV_i and described by

$$S(\omega) = \begin{cases} A_0^2/\omega & \text{for } \omega_{\text{ir}} \leq \omega \leq \omega_{\text{cutoff}} \\ A_0^2\omega_{\text{cutoff}}/\omega^2 & \text{for } \omega_{\text{cutoff}} \leq \omega \leq \infty \end{cases} \quad (7)$$

where A_0 is the noise strength at 1Hz. Using an estimate $A_0 = 1\mu\text{V}$, $\omega_{\text{cutoff}} = 100\text{MHz}$ [33] and $\omega_{\text{ir}} \approx 10^{-3}\text{Hz}$ for

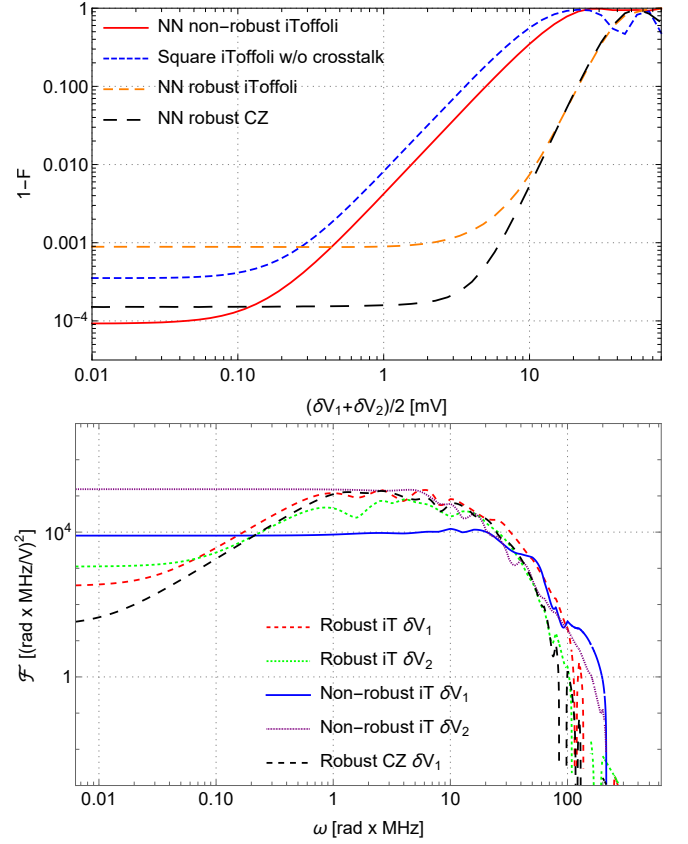


FIG. 4. Top: Trace infidelity of the gates vs quasistatic fluctuations in average barrier voltage $(\delta V_1 + \delta V_2)/2$. Bottom: Filter function of the neural-network designed gates for barrier gate fluctuations δV_1 and δV_2 .

both voltages results in an estimated infidelity as a result of frequency dependent charge noise of 8.4×10^{-3} for the robust CZ gate.

C. iToffoli gate

Now we turn to the main results of this work. The control fields for the non-robust and robust iToffoli gates are shown in Figs. 5 and 6. The non-robust iToffoli was implemented in a gate time of $8.5\pi/J_{\text{max}}$ and a peak driving amplitude of $\Omega = 0.71/J_{\text{max}}$, which is less than the imposed constraint $\Omega \leq \Omega_{\text{max}} = 10\text{MHz}$. The robust iToffoli used a gate time of $2\pi/J_{\text{max}}$ and saturated the amplitude constraint.

1. Charge noise analysis

The effect of charge noise is analyzed in the way described in section III B 1. In the quasistatic case, we obtain an infidelity below 10^{-3} for average voltage fluctuations of 0.4mV for the non-robust pulse and 2.1mV for the robust pulse as shown in Fig. 4. To analyse the

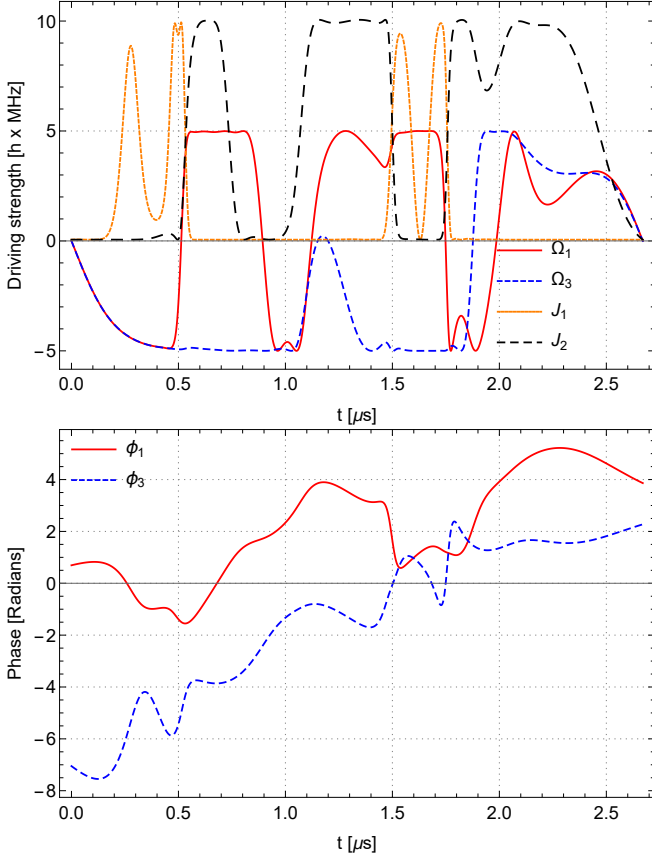


FIG. 5. Neural network designed control fields vs time for a non-robust iToffoli gate in the presence of crosstalk. Top: Exchange amplitudes J_1 and J_2 as well as driving tone amplitudes Ω_1 and Ω_3 . Bottom: Accompanying phase modulation of the driving tones ϕ_1 and ϕ_3 .

$1/f$ frequency dependent charge noise, the filter function formalism was applied again. The filter functions for both the robust and non-robust neural network designed iToffoli gates, \mathcal{F}_i , are plotted in Fig. 4. Using the same estimates of $A_0 = 1\mu V$, $\omega_{\text{cutoff}} = 100\text{MHz}$ [33] and $\omega_{\text{ir}} \approx 10^{-3}\text{Hz}$ for both voltages results in an estimated infidelity as a result of frequency dependent charge noise of 1.6×10^{-2} for the robust iToffoli, compared to 9.4×10^{-2} for the non-robust iToffoli. The robust iToffoli infidelity is almost an order of magnitude lower and this ratio would also be maintained for devices designed to have smaller charge noise strengths [34].

2. Bandwidth and time lengths

When considering the pulses discussed above to mitigate charge noise, one might worry that the bandwidth of the control hardware and time length to implement the pulses can limit their usefulness. However, the robust iToffoli requires a 3dB bandwidth of only 1.5MHz to implement and the non-robust iToffoli requires a 3dB bandwidth of 2.8MHz. The robust iToffoli gate uses less

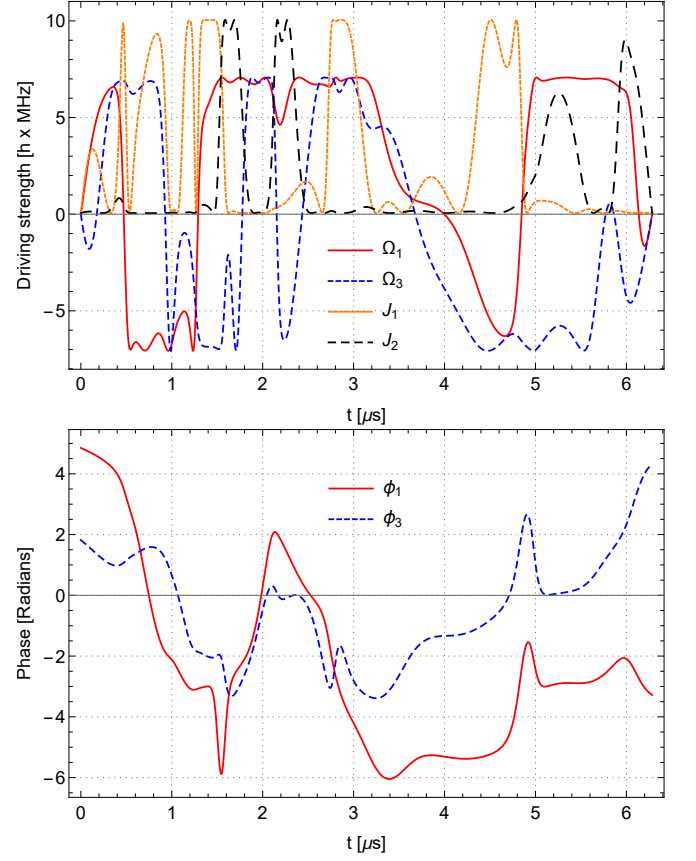


FIG. 6. Neural network designed control fields vs time for charge noise robust iToffoli gate in the presence of crosstalk. Top: Exchange amplitudes J_1 and J_2 as well as driving tone amplitudes Ω_1 and Ω_3 . Bottom: Accompanying phase modulation of the driving tones ϕ_1 and ϕ_3 .

bandwidth than its non-robust counterpart most likely because the non-robust iToffoli is carried out on a shorter timescale. These bandwidths are easily achievable in experiments, where the fast control lines can have bandwidths (after a low-pass filter) on the order of 200MHz [35].

The total time of the non-robust iToffoli pulse is $8.5\pi/J_{\text{max}} \approx 26.7/J_{\text{max}}$ which is only slightly longer than the previously known iToffoli gate for the case where crosstalk is not an issue [13], which is approximately $20.6/J_{\text{max}}$ long. The length of the generated pulse is hard to compare to a Toffoli gate synthesized using one- and two-qubit gates in this three-qubit system with large crosstalk. This is because there is no straightforward way to perform the individual one- and two-qubit gates unless a similar numerical optimization is performed for each step. But to get a rough (and overly conservative) estimate, we can compare to the length of a synthesized Toffoli gate using a three-qubit system *without* appreciable crosstalk. Using the same maximum driving and exchange amplitudes as in the optimization, the standard Toffoli gate synthesized as shown in Fig. 7 will take $\approx 34.4/J_{\text{max}}$ if virtual-z gates are used. This is slower

- [16] I. Heinz and G. Burkard, Phys. Rev. B **104**, 045420 (2021).
- [17] P. Huang, N. M. Zimmerman, and G. W. Bryant, npj Quantum Inf **4**, 62 (2018).
- [18] J. van Dijk, E. Kawakami, R. Schouten, M. Veldhorst, L. Vandersypen, M. Babaie, E. Charbon, and F. Sebastiano, Phys. Rev. Applied **12**, 044054 (2019).
- [19] U. Güngördü and J. P. Kestner, Phys. Rev. B **101**, 155301 (2020).
- [20] U. Güngördü and J. P. Kestner, Phys. Rev. Research **4**, 023155 (2022).
- [21] D. W. Kanaar, U. Güngördü, and J. P. Kestner, Phys. Rev. B **105**, 245308 (2022).
- [22] D. C. McKay, C. J. Wood, S. Sheldon, J. M. Chow, and J. M. Gambetta, Phys. Rev. A **96**, 022330 (2017).
- [23] D. Loss and D. P. DiVincenzo, Phys. Rev. A **57**, 120 (1998).
- [24] T. F. Watson, S. G. Philips, E. Kawakami, D. R. Ward, P. Scarlino, M. Veldhorst, D. E. Savage, M. G. Lagally, M. Friesen, S. N. Coppersmith, M. A. Eriksson, and L. M. Vandersypen, Nature **555**, 633 (2018), 1708.04214.
- [25] X. Croot, X. Mi, S. Putz, M. Benito, F. Borjans, G. Burkard, and J. R. Petta, Phys. Rev. Research **2**, 012006 (2020).
- [26] B. Undseth, X. Xue, M. Mehmandoost, M. Russ, P. T. Eendebak, N. Samkharadze, A. Sammak, V. V. Dobrovitski, G. Scappucci, and L. M. K. Vandersypen, (2023), arXiv:2205.04905 [cond-mat.mes-hall].
- [27] W. Gilbert, T. Tanttu, W. H. Lim, M. Feng, J. Y. Huang, J. D. Cifuentes, S. Serrano, P. Y. Mai, R. C. C. Leon, C. C. Escott, K. M. Itoh, N. V. Abrosimov, H.-J. Pohl, M. L. W. Thewalt, F. E. Hudson, A. Morello, A. Laucht, C. H. Yang, A. Saraiva, and A. S. Dzurak, Nat. Nanotechnol. **18**, 131 (2023).
- [28] C. Rackauckas, M. Innes, Y. Ma, J. Bettencourt, L. White, and V. Dixit, (2019), arXiv:1902.02376 [cs.LG].
- [29] C. Rackauckas and Q. Nie, The Journal of Open Research Software **5**, 15 (2017).
- [30] J. M. Boter, X. Xue, T. Krähenmann, T. F. Watson, V. N. Premakumar, D. R. Ward, D. E. Savage, M. G. Lagally, M. Friesen, S. N. Coppersmith, M. A. Eriksson, R. Joynt, and L. M. K. Vandersypen, Phys. Rev. B **101**, 235133 (2020).
- [31] T. Meunier, V. E. Calado, and L. M. K. Vandersypen, Phys. Rev. B **83**, 121403 (2011).
- [32] T. J. Green, J. Sastrawan, H. Uys, and M. J. Biercuk, New J. Phys. **15**, 095004 (2013).
- [33] E. J. Connors, J. Nelson, H. Qiao, L. F. Edge, and J. M. Nichol, Phys. Rev. B **100**, 165305 (2019).
- [34] B. Paquelet Wuetz, D. Degli Esposti, A.-M. J. Zwerver, S. V. Amitonov, M. Botifoll, J. Arbiol, L. M. K. Vandersypen, M. Russ, and G. Scappucci, Nat. Commun. **14**, 1385 (2023).
- [35] X. Xue, B. Patra, J. P. G. van Dijk, N. Samkharadze, S. Subramanian, A. Corna, B. Paquelet Wuetz, C. Jeon, F. Sheikh, E. Juarez-Hernandez, B. P. Esparza, H. Rampurawala, B. Carlton, S. Ravikumar, C. Nieva, S. Kim, H.-J. Lee, A. Sammak, G. Scappucci, M. Veldhorst, F. Sebastiano, M. Babaie, S. Pellerano, E. Charbon, and L. M. K. Vandersypen, Nature **593**, 205 (2021).